SAPP XXII

22nd Symposium on Application of Plasma Processes and 11th EU-Japan Joint Symposium on Plasma Processing

Book of Contributed Papers

Štrbské Pleso, Slovakia
18-24 January, 2019

Edited by V. Medvecká, J. Országh, P. Papp, Š. Matejčík

Book of Contributed Papers: 22nd Symposium on Application of Plasma Processes and 11th EU-Japan Joint Symposium on Plasma Processing, Štrbské Pleso, Slovakia, 18-24 January 2019.

Symposium organised by Department of Experimental Physics, Faculty of Mathematics, Physics and Informatics, Comenius University in Bratislava and Society for Plasma Research and Applications in hotel SOREA TRIGAN***, Štrbské Pleso, Slovakia, 18-24 January 2019.

Editors: V. Medvecká. J. Országh, P. Papp, Š. Matejčík

Publisher: Department of Experimental Physics, Faculty of Mathematics, Physics and Informatics, Comenius University in Bratislava; Society for Plasma Research and Applications in cooperation with Library and Publishing Centre CU, Bratislava, Slovakia

Issued: January 2019, Bratislava, first issue

Number of pages: 386

URL: http://neon.dpp.fmph.uniba.sk/sapp/

CHEMICAL KINETIC MODEL OF TRANSIENT SPARK: SPARK PHASE AND NO_X FORMATION

Mário Janda, Karol Hensel, Zdenko Machala

Division of Environmental physics, Faculty of Mathematics, Physics and Informatics, Comenius University, Mlynská dolina F2, 842 48 Bratislava, Slovakia
E-mail: janda@fmph.uniba.sk

Transient Spark (TS) discharge generated in atmospheric air is an efficient source of NO_x for biomedical applications with a negligible O_3 production. The TS discharge is characteristic by short (~10 ns) and high current (~A) spark pulses initiated by streamers. The paper presents chemical kinetic model of the TS that simulates electron density evolution during both streamer and spark phases and studies generation of selected reactive oxygen and nitrogen species (RONS), e.g. O, N, NO, NO_2, and O_3, that are important for their antibacterial and other biomedical effects. The dominant intermediate product of the streamer chemistry is atomic O. Without the following spark phase, this would lead to the generation of O_3 as the dominant final product. In the spark phase, unlike in the streamer phases, the chemistry is twisted towards production of reactive nitrogen species (RNS), as the density of N atoms exceeds the atomic O density. This is in agreement with the experimental observation that TS generates more NO_x than O_3, although the generation of NO_x occurs mainly during the relaxation phase following the TS pulse, which is not yet included in the presented model.

1. Introduction

The transient spark (TS) is a dc-operated, self-pulsing and filamentary discharge with typical repetition frequency in the range 1-10 kHz. Fundamental research of the positive polarity TS revealed that it is characteristic by the short (~10-100 ns) spark current pulses, having maximum amplitude in the range of a few Amps [1]. Thanks to the short spark pulse duration and limited amount of deposited energy (~1 mJ/pulse), significant heating of the treated gas is avoided and the generated plasma is non-equilibrium and highly reactive, with the electron density above 10^{17} cm^{-3} [2].

The reactive plasma properties predetermine the TS for environmental and biomedical applications or generation of nanoparticles [3, 4]. In biomedical applications, the major antibacterial role in TS discharge is attributed to reactive oxygen and nitrogen species (RONS) [5]. We recently reported the efficient generation of nitrogen oxides (NO_x) by TS discharge [6]. The NOx production rate ~7×10^{16} molecules/J was achieved. We assume that further optimization of NO_x formation by TS is also possible. It requires further study of TS including its chemical kinetic modeling.

The modeling of chemical kinetics aiming to calculate the temporal density evolution of all species included in the kinetic model is an effective tool for plasma chemistry [7-10]. It is commonly used not only for the modeling of cold plasma chemistry including RONS generation [7], but also for the description of high-temperature steady-state arc plasmas [8], nanosecond duration of streamer propagation [9], or fast gas heating in pulsed discharges [10]. The chemical kinetic modeling could also help us to better understand the TS discharge physical and chemical characteristics.

We presented a chemical kinetic model developed for TS discharge with a focus on the initial streamer phase recently [11]. Here we present an updated version of this model including the spark phase. The validity of the model was tested by comparing the calculated electron density with experimental data [2]. This model is further used to analyse the generation of selected RONS: O, N, O_3, NO, and NO_2.

2. Transient Spark

Figure 1 shows a schematic of the electric circuit used to generate the positive TS discharge by a positive polarity dc high-voltage (HV) power supply connected to a metal needle HV electrode via a series resistor (R = 5-10 MΩ). In the same way, the negative TS can be generated using negative dc HV power supply [12]. The usual distance d between the tip of the HV electrode and a grounded electrode is 4-10 mm. For the grounded electrode we typically use plate, mesh, or blunt tip.

The TS is initiated by a streamer current pulse with the amplitude 50-100 mA (blue dots in Fig. 2, top-right corner), appearing when the potential on the stressed electrode reaches the voltage V_{TS} characteristic for the TS discharge. The optical visualization of the TS temporal evolution revealed two events during the initial TS phase, identified as primary and secondary streamers [13, 14]. The primary streamer creates a relatively conductive plasma bridge between the electrodes. This enables partial discharging of the internal capacitance C of the electric circuit generating TS, and heating of the gas inside this plasma channel during the streamer-to-spark transition phase. The spark current pulse appears when the gas temperature inside the plasma channel increases up to ~1000 K [15].

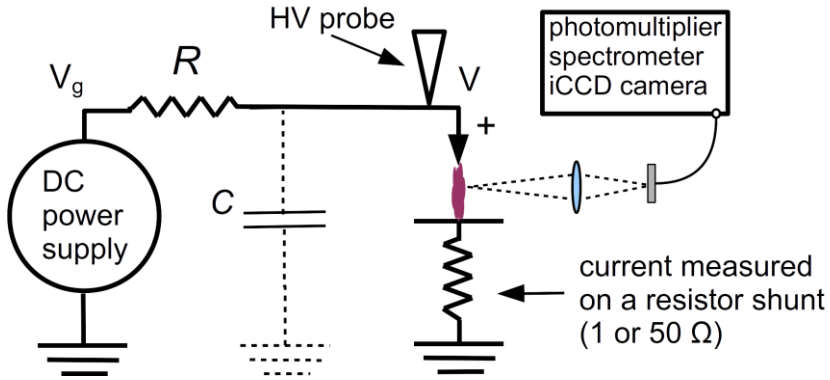

Fig. 1. Schematic of the set-up used for generation and diagnostics of the TS.

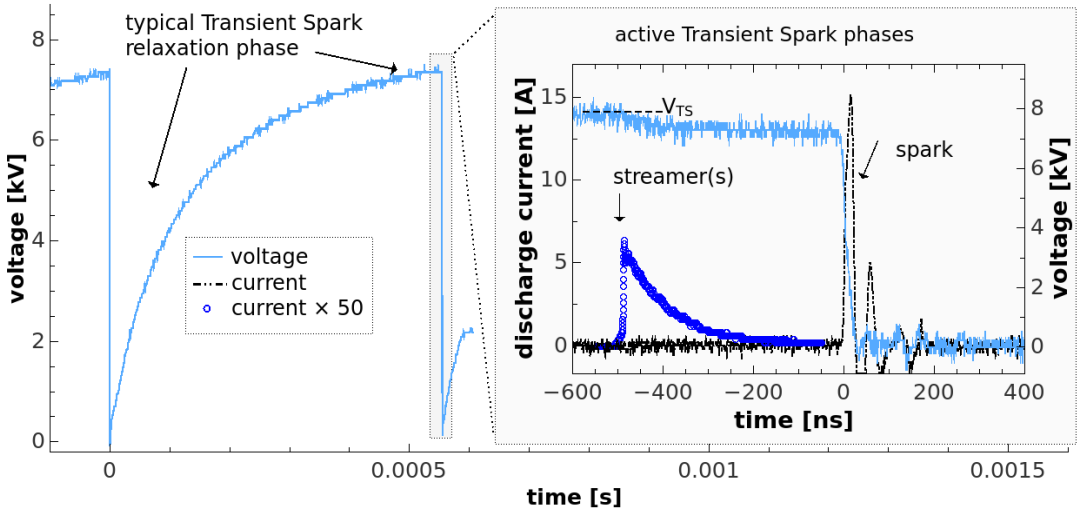

Fig. 2. Typical voltage and current waveforms of the TS.

During the spark phase, the electric circuit internal capacitance discharges completely, the voltage on the HV electrode drops to almost zero, and the discharge current reaches a high value (~1-10 A) for a short time. The electron density n_e during the TS spark phase can exceed 10^{17} cm^{-3} [2]. The gas temperature in the plasma channel shortly after the spark increases to at least 1500-3500 K [6]. However, complete thermalization of plasma is most probably not possible due to small amount of energy stored in C that is delivered to the gap during the spark phase.

The large ballast resistor R limits the dc current delivered to the plasma after the spark current pulse when C is discharged. As a result, the plasma starts to decay after the spark pulse. Eventually, the plasma resistance exceeds R and the potential V on the stressed electrode gradually increases (long time scale voltage waveform in Fig. 2), as the capacitance C recharges during the TS relaxation phase. A new TS pulse, initiated by a new streamer, occurs when V reaches again the characteristic voltage V_{TS}. The TS is thus based on repetitive charging and discharging of C. The repetition frequency f of this process can be controlled by generator voltage V_g approximately in the range 1-10 kHz [1].

3. Model Description

The aim of the chemical kinetic model is to calculate density evolution of studied species interacting via defined set of chemical reactions. For this purpose we used ZDPlasKin software code [16]. Authors of ZDPlasKin also provide a ready-to-use list of chemical processes in N_2-O_2 plasmas with all necessary rate coefficients. We used this set of reactions (version 1.03) in our simulations too. This set includes ~650 chemical reactions for 53 species, namely, molecules N_2 (X^1, v = 0-8), N_2 (A^3, B^3, a'^1, C^3), O_2 (X^3, v = 0-4), O_2 (a^1, b^1, 4.5 eV), O_3, NO, N_2O, NO_2, NO_3 and N_2O_5, atoms N (^4S, ^2D, ^2P) and O (^3P, ^1D, ^1S), positive ions N^+, N_2^+, N_3^+, N_4^+, O^+, O_2^+, O_4^+, NO^+, N_2O^+, NO_2^+ and $O_2^+N_2$, negative ions O^-, O_2^-, O_3^-, O_4^-, NO^-, N_2O^-, NO_2^- and NO_3^-, and electrons. The electron impact excitation of other electronic states of nitrogen is also included, but the model assumes their instantaneous relaxation: $N_2(W^3, B'^3) \rightarrow N_2(B^3)$; $N_2(a^1, w^1) \rightarrow N_2(a'^1)$, and $N_2(E^3, a''^1) \rightarrow N_2(C^3)$. The generalized level O_2(4.5 eV) corresponds to $O_2(A^3, C^3)$ and $O_2(c^1)$ states.

The rate constants of reactions between heavy species are specified in the input file. The rate constants for electron impact reactions are calculated from electron energy distribution function (EEDF). The ZDPlasKin module enables to use either Maxwellian distribution functions defined by the electron temperature T_e, or the EEDF obtained by solving the Boltzmann equation for free electrons. The ZDPlasKin package includes a Bolsig+ solver [17] for this purpose. A set of required electron scattering cross sections was taken from the LXCat project database [18].

Finally, ZDPlasKin module requires to use additional subroutines for more comprehensive control of simulation conditions, e.g. changes in the gas temperature and reduced electric field. Our major goal was to create a module compatible with ZDPlasKin with subroutines that would take into account fast changes in the reduced electric field strength E/N, gas temperature T_g, electron temperature T_e and total density of neutrals N characteristic for a TS discharge. The time evolution of E/N, T_g, T_e and N simulating the TS were constructed based on our experimental results and the literature, as it is explained in the next sections.

3.1. Streamer phase

The streamer phase is relatively short (<200 ns) initial phase of the TS discharge consisting of the primary and the secondary streamer. The streamer phase of the TS is mainly characterized by fast changes of E/N. It is therefore necessary to determine the density of many species that could influence the plasma induced chemistry with good temporal resolution (~ns), while processes such as diffusion can be neglected on this short time scale.

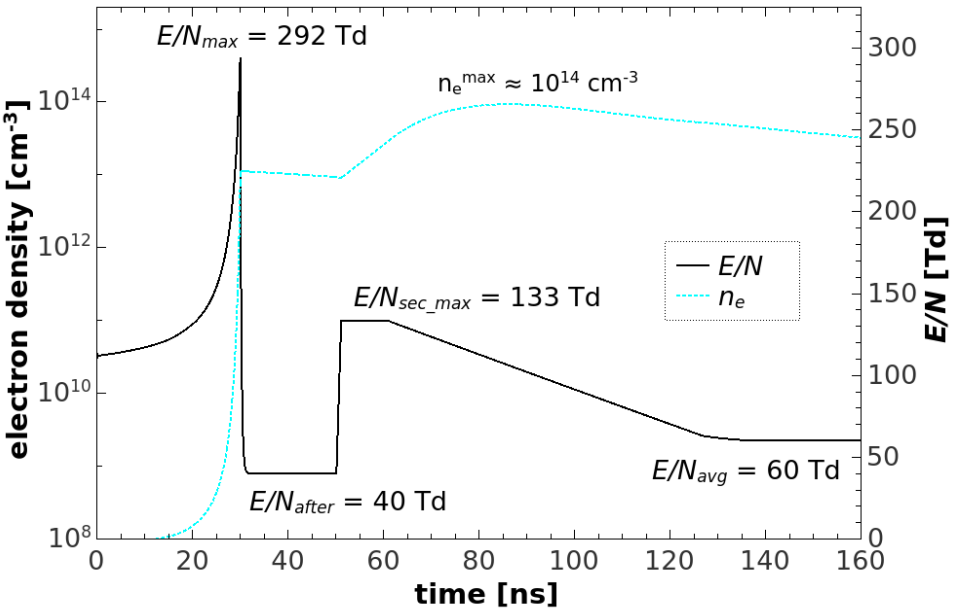

Fig. 3. The modeled reduced electric field strength profiles and calculated electron density during the primary and the secondary streamer phase of the TS discharge.

The influence of the primary and the secondary streamer on the rates of chemical reactions in our 0-D kinetic model can be introduced by using appropriate temporal evolution of *E/N*. The temporal evolution of *E/N* used in our model (Fig. 3) is based on published primary and secondary streamer characteristics and our experimental results (see [11] and references therein). The aim was to achieve the peak electron density during the TS streamer phase close to the experimentally observed $n_e \approx 10^{14}$ cm^{-3} [2].

3.2 Streamer-to-spark transition phase

An average streamer-to-spark transition time τ depends strongly on TS repetition frequency *f*. At lower frequencies (< 3 kHz), τ is very random and it can vary from a few hundred ns up to several μs [15]. With increasing frequency, τ drops below ~100 ns and at ~10 kHz, we even observed an almost instantaneous formation of a spark after the streamer [13]. Here we study "low" frequency TS (~1 kHz), where the streamer and spark current pulses are well separated, and the current before the spark falls down to a few mA [15].

Decrease of the current and n_e (Fig. 3) results from relatively low E/N_{avg} = 60 Td in the plasma channel established after the disappearance of the secondary streamer. Transition to the spark requires the increase of *E/N* to accelerate the ionization processes. In TS, it can be achieved only by the significant decrease in *N*. We thus assume that the breakdown and spark formation in TS at low frequencies proceeds via mechanism postulated by Marode et al. [19]. It can be summarized as follows: heating of the channel → increase in the pressure → hydrodynamic expansion → decrease in *N* in the core of the channel → increase in *E/N* → acceleration of ionization processes → gas breakdown.

We are not able to calculate the time evolution of gas density *N(t)* with our 0-D kinetic model. For this reason, we tested the *N* profile (Fig. 4) from the simulations of Naidis [20]. Besides the hydrodynamic expansion, it also handles the radial diffusion of particles from the discharge channel. We suppose that this profile is the closest match to the TS discharge we found in the literature.

The changes of *N* according to the profile taken from Naidis starts in the calculation time 650 ns, so that the fastest rate of *N* decrease is reached in the moment when T_g = 1000 K (Fig. 4, calculation time 800 ns). We extrapolated this profile and the *N* starts to decrease from initial N_o (≈ 2.09×10^{19} cm^{-3} for initial gas temperature T_g^{ini} = 350 K at atmospheric pressure) already after the primary streamer (from the calculation time 40 ns). The rate of the extrapolated gas density decrease is proportional to the difference between the T_g and T_g^{ini}. The T_g increases linearly during the calculation time 40 ns to 800 ns from T_g^{ini} to 1000 K. The temperature remains constant for very short time till the end of the streamer-to-spark transition phase.

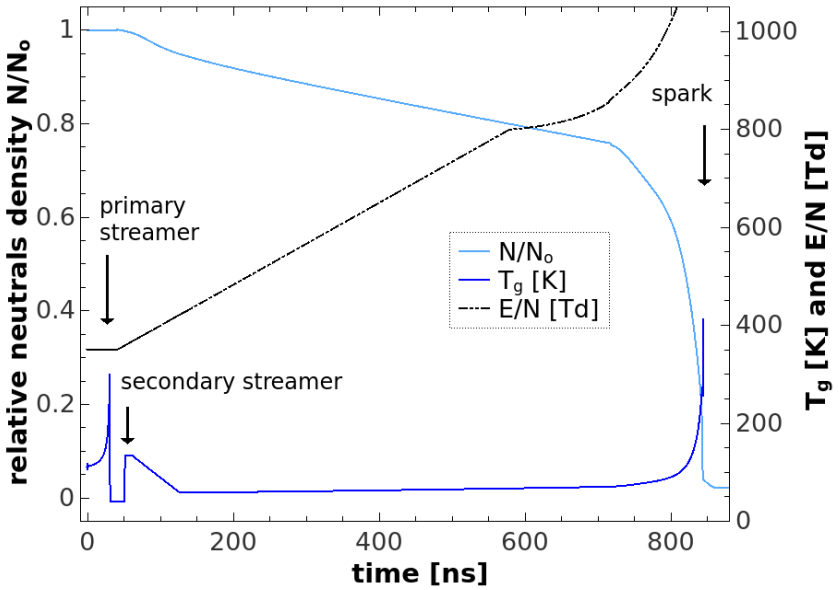

Fig. 4. The evolution of reduced electric field strength *E/N*, gas temperature T_g and relative density of heavy particles N/N_o during the streamer-to-spark transition phase used in model.

The streamer-to-spark transition phase in our model stops when the ionization degree ξ reaches 2×10^{-2} We use this limit because the Bolsig+ solver can reliably calculate EEDFs and rate of electron-molecule impact processes only for $\xi < 2\times10^{-2}$. We calculate ξ as

$$\zeta = \frac{n_e}{n_e+N+N_{ion}}, \tag{2}$$

where N_{ion} is the density of ions.
For calculation of *E/N* required by Bolsig+ solver, we must also calculate the evolution of the electric field *E* inside the plasma channel. First, our model calculates the time evolution of potential *V(t)* between the electrodes. We actually simulate the discharging of *C* via the plasma resistance R_p. The advantage of this approach is that besides n_e, we calculate another variable that can be compared with experimental data: *V(t)*.
The decrease in potential ΔV^i for the i-th calculation step can be expressed as

$$\Delta V^i = -V^{i-1}\times\frac{\Delta t}{C R_p^{i-1}}. \tag{3}$$

The R_p is related to the plasma conductivity σ_p by

$$R_p = \frac{4d}{\sigma_p \pi D_p^2}, \tag{4}$$

where d and D_p are the plasma channel length and the diameter, respectively. For approximation of D_p we used the experimentally obtained value defined as the full-width at half-maximum of the spectrally unresolved radial intensity profile of the plasma channel after the Abel inversion [2]. At low TS repetition frequencies (below 4 kHz), we observed shrinking of the discharge channel diameter during the streamer-to-spark transition from $D_p^{\text{streamer}} \approx 150 \pm 40$ μm in the streamer phase, down to $D_p^{\text{spark}} \approx 50 \pm 20$ μm in the spark phase.
The plasma conductivity σ_p is calculated by the model from n_e

$$\sigma_p = \frac{e^2 n_e}{m_e \nu_m}. \tag{5}$$

Here e and m_e are the electron charge and mass, respectively, and ν_m is the effective collision frequency of electrons with heavy particles, provided by Bolsig+ solver. Finally, *E/N(t)* is derived from *V(t)* and *N(t)* assuming homogeneous axial potential distribution.

3.3 Spark phase

The spark phase in our model starts when the ionization degree ξ reaches 2×10^{-2} and it continues to increase further. Unlike in the previous phases, plasma is thus highly ionized. The duration of the spark phase in our model can be defined in the configuration files. We used 400 ns duration, as we found it is long enough for plasma to become weakly ionized again. On the other side, we assume that it is short enough to neglect processes such as diffusion or mixing with the surrounding air during this phase.
Thanks to the high degree of ionization we can use Maxwellian EEDFs during the spark phase. The usage of Bolsig+ solver is not preferable because of the high degree of ionization, but also because of high degree of atomization during this phase. The available sets of electron scattering cross sections for O and N atoms are simply not adequate to calculate EEDFs accurately. Using Maxwellian EEDFs, the knowledge of the *E/N* evolution is not important anymore and thus also the evolution of *N* is not crucial unlike in the previous phase when we rely on *N* evolution taken from external source [20]. Fur-

ther evolution of N during the spark phase is handled by our model itself, i. e. the density of neutrals changes only via chemical processes.
The crucial parameter during the spark phase is the electron temperature that defines the Maxwellian EEDF. We calculate T_e from the mean electron energy ε. The evolution of ε is calculated numerically starting from the last value calculated by Bolsig+ solver at the end of the streamer-to-spark transition phase using electron energy balance equation [21]

$$\frac{d\varepsilon}{dt} = \frac{e^2 E^2}{m_e \nu_m} - \delta(\varepsilon - \varepsilon_g)\nu_m \quad . \tag{6}$$

The first term on the right side represents the energy gained from the electric field; the second term represents the energy losses due to collisions with heavy particles having mean energy ε_g. The collision frequency ν_m includes collisions of electrons with both neutrals and ions, and the coefficient δ determines relative amount of energy lost per single collision.
If we take into account only elastic collisions, then $\delta = \delta_e = 2m_e/M_{avg}$, where M_{avg} is a weighted average mass of heavy particles. Since $m_e << M_{avg}$, the typical value of δ_e is only ~5×10^{-5}. This explains why elastic collisions do not efficiently transfer energy from electrons to heavy particles in weakly ionized plasma. Our model takes into account inelastic collisions of electrons when calculating δ, therefore this parameter is much higher before the spark phase (~10^{-2}). The δ decreases in strongly ionized plasma with high frequency of elastic electron-ion collisions, which are characterized by large coulomb cross sections. In our simulations we can see this situation in Figure 5 in calculation time 850-900 ns. Here δ drops down to ~10^{-4} and there is a peak of ν_m due to increasing amount of electron-ion collisions.
Later (calculation time >1000 ns), δ slightly increases but it remains relatively low despite decreasing degree of ionization. This is due to gas composition changes. Molecules with many vibrational levels consuming lot of energy decompose to O and N atoms. In highly atomized gas, the vibrational excitation processes are negligible and δ can be increased only by electronic excitations and ionizations of atoms. Unfortunately, we lack electron scattering cross sections for most excitation levels of O and N atoms. Therefore, the parameter δ is probably underestimated in our model when gas is highly atomized. However, it is probably not crucial for calculation of δ, because the mean energy of electrons is relatively low in this phase (~1 eV), and the excitation probability of higher energy levels is thus low.

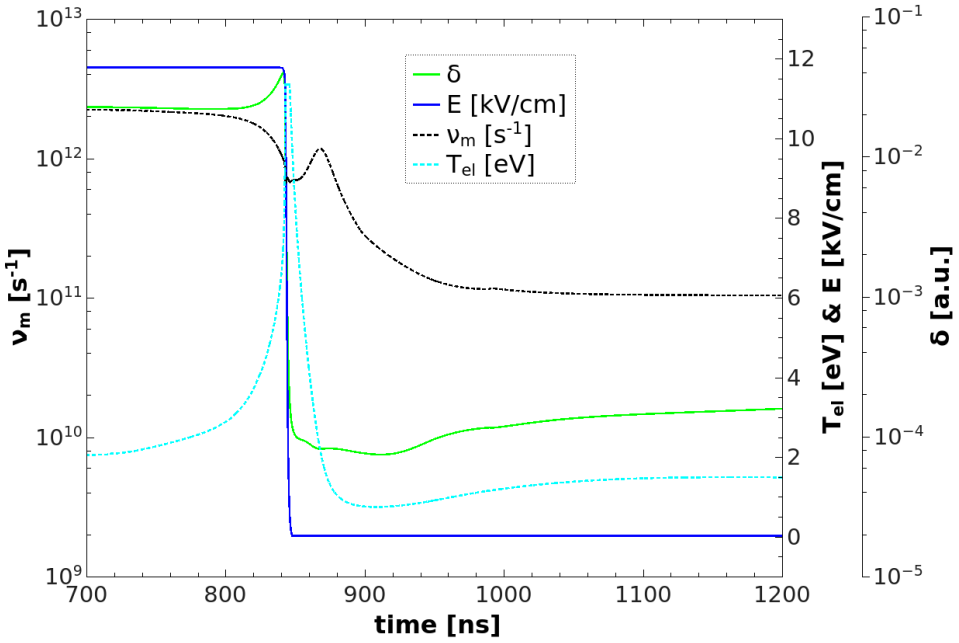

Fig. 5. The evolution of electric field E, electron temperature T_e, electron collision frequency and relative energy loss per collision δ during the spark phase used in the model.

The electric field evolution *E(t)* during the spark phase is derived from calculated *V(t)* similarly as it is done with *E/N(t)* during the streamer-to-spark transition phase (see section 3.2, eq. 3-5). The main differences is that *V(t)* changes slowly during the streamer-to-spark transition phase, while it drops quickly to almost zero during the spark phase. Since spark can be considered as an arc discharge with short duration, we decided to stop the voltage drop in our model in the moment when *V* reaches minimal voltage V_{min} = 40 V, characteristic for an arc discharge [21]. We further subtract 25 V from V_{min} when calculating *E*, taking into account typical cathode and anode fall voltages.
The fast drop of *E* when plasma becomes strongly ionized is accompanied by almost equally fast decrease of δ (Fig. 5). The electron temperature T_e decreases to ~1 eV within ~40 ns. The fast decrease of T_e means a fast transfer of energy to heavy particles, i.e. gas heating. In our model, the gas temperature during this short period (initial 40 ns of the spark phase) increases exponentially from 1000 K to 3000 K. Later, when T_e drops to ~1 eV and δ is low, the energy transfer from electrons to heavy particles should be also much slower. For this reason we also slowed down further increase of T_g, from exponential growth to logarithmic-like growth from 3000 K up to 3500 K at the end of the spark phase. The T_g = 3500 ± 500 K was the highest temperature observed experimentally in TS.

4. RONS Generation

The presented model reasonably calculates voltage drop during the spark phase. More important is that a good agreement was achieved (Fig. 6) when comparing the calculated electron densities with experimental data [1, 2]. We thus assume that this model can be used to determine reliably the density evolution of various species, which we are not able to measure using available experimental techniques. Next, we focus on temporal evolution of the selected RONS, namely NO, NO_2, N, O, and O_3.

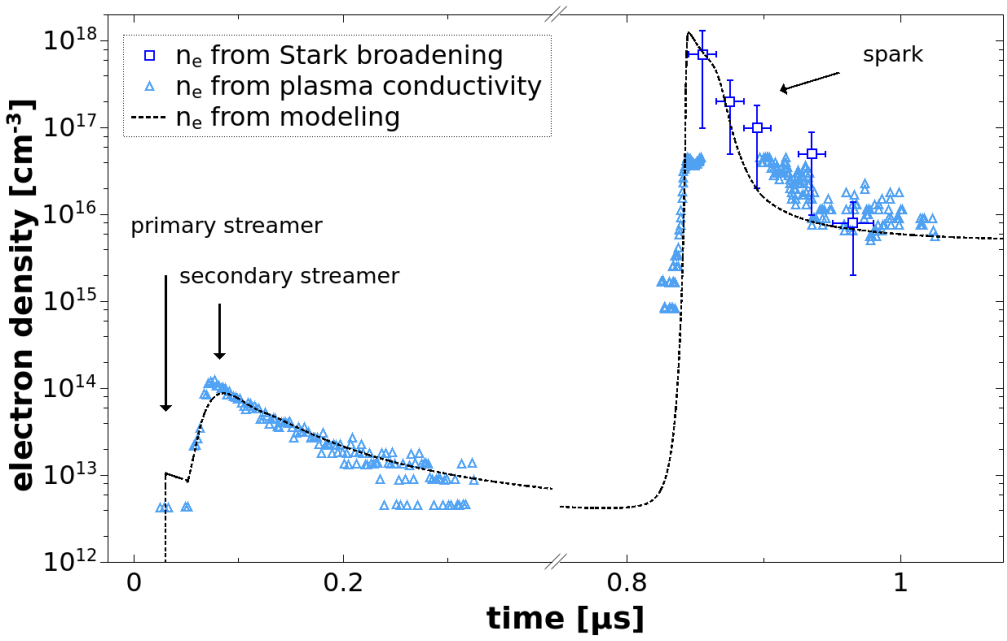

Fig. 6. Comparison of the measured and calculated electron density.

4.1. Evolution of RONS before the spark phase

Each TS spark pulse is initiated by the primary streamer propagating from the HV electrode towards the grounded electrode with strong electric field in its head. With *E/N* ≈ 300 Td, electrons gain high energy and are able to initiate various chemical processes. During the secondary streamer phase, the field is lower, but the duration of the secondary streamer is longer and therefore higher electron density is achieved (Fig. 6). For this reason, the secondary streamer strongly influences the density of produced reactive species (Fig. 7). Later, during the streamer-to-spark transition phase, the changes of selected RONS densities are relatively slow.

The density of NO is higher than the density of O_3 before the spark phase, and the NO_2 density is even lower than O_3. However the density of atomic O is the highest among the reactive species and this indicates that NO must be converted to NO_2 in later phases. We really observed this process when we simulated a hypothetical situation with primary and secondary streamer phases but no spark phase [11]. More importantly we observed that the final dominant product was ozone, since the atomic O density after the streamer phase highly exceeded the density of atomic N. Thus, only the following spark and relaxation phases can explain why the TS generates preferentially NO_x and not O_3 [6].

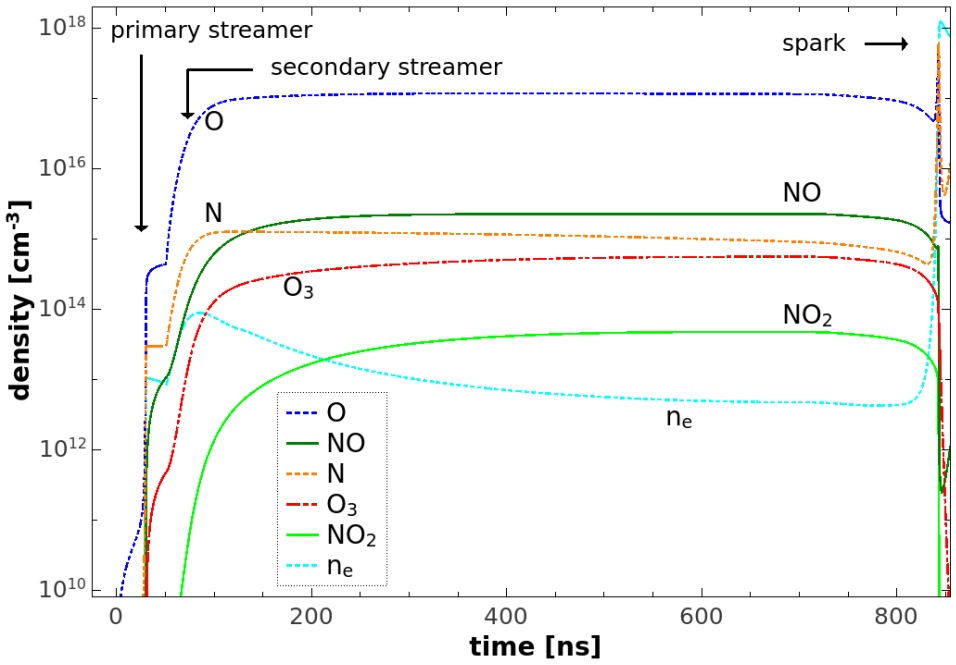

Fig. 7. Calculated densities of electrons and selected RONS before transition to spark.

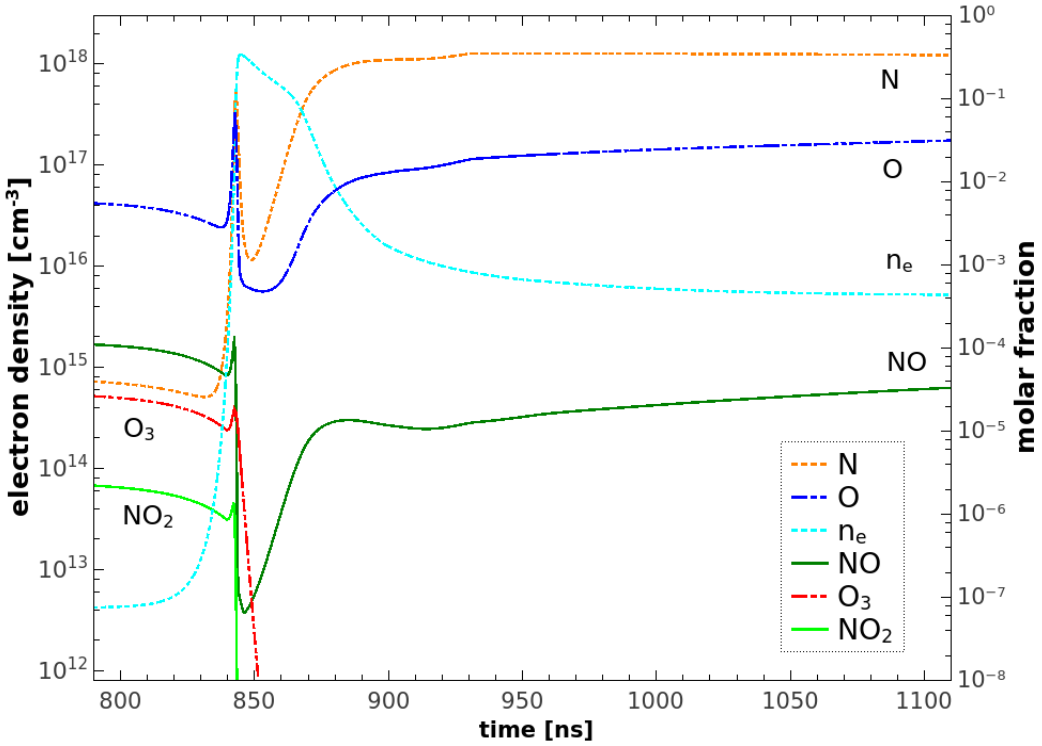

Fig. 8. Calculated electron density and molar fraction of selected RONS during the spark phase.

4.2. Evolution of RONS during the spark phase

The spark pulse in our model is induced by the gas density decrease causing the increase of *E/N* and T_e. The densities of all neutrals thus change due to two different processes, chemical reactions and hydrodynamic expansion simulated by the decrease of *N*. In order to show only the changes due to chemical processes, we present here evolution of molar fractions of studied RONS during the spark phase (Fig. 8).

The spark phase is characterized by a strong increase of ionization degree, gas temperature and decomposition of molecules. The dissociation degree of three-atomic molecules (NO_2, O_3) is approximately by two orders of magnitude higher than the dissociation of two-atomic molecules such as NO. However, even the molar fraction of NO decreases by three orders of magnitude during the initial part of the spark phase. Thus, we can say that NO, NO_2 and O_3 densities achieved during the previous streamer phase have almost no influence on the final densities of these species. Their final densities will be established later during the relaxation phase, which is not included in the model yet. During the spark phase, we mostly see generation of their precursors: N and O atoms. Unlike in the previous phases, the amount of N exceeds the amount of O atoms during the spark phase (Fig. 8). This is the first indicator of the experimentally observed result that TS generates more NO_x than O_3.

5. Conclusions

The transient spark (TS) discharge has been successfully used for various biomedical and environmental applications. The TS can be used as relatively cheap and simple NO_x generator, however its further optimization requires better understanding of basic chemical processes that take place during different phases of the TS. Therefore, we studied TS discharge using chemical kinetic modeling. The 0-D model based on ZDPlasKin module was successfully used to model plasma induced chemistry during the transient events propagating in space, such as primary and secondary streamers. The ZDPlasKin was also used to model plasma chemistry during the spark phase characterized by highly ionized non-thermal plasma. The electron density calculated in our model agrees well with experimental observations.

We further focused on the production of selected RONS playing important roles in biomedical applications of electrical discharges in air: O, N, NO, NO_2 and O_3.We found out that the secondary streamer strongly influences the densities of these reactive species. The density of NO is higher than the density of O_3 shortly after the secondary streamer. However, the density of atomic O after the secondary streamer is even higher than NO and O_3 densities, and it strongly exceeds the density of atomic N. When we simulated a hypothetical situation with primary and secondary streamer phases but no spark phase, the final dominant product was O_3. In transient spark, however, the experimental data shows that NO_x are dominant products and there is no O_3. We assume that this results from the enhancement of atomic N generation and gas heating during the spark phase. Our model shows that the amount of N exceeds the amount of O atoms during the spark phase. Due to the strong degree of atomization during the spark phase, the densities achieved during the streamer phase has almost no influence on the final densities of NO, NO_2 and O_3.

Our results indicate that the production of stable products NO, NO_2 and O_3 determining their final densities must occur later, during the TS relaxation phase. We are planning further development of our kinetic model to be able to reliably simulate the relaxation phase of the TS discharge to prove this hypothesis and find better correlation with experiments.

Acknowledgement: This work was supported by Slovak Research and Development Agency APVV-17-0382, and Slovak Grant Agency VEGA 1/0419/18.

6. References

[1] Janda M et al. 2011 *Plasma Sources Sci. Technol.* **20** 035015.
[2] Janda M et al. 2014 *Plasma Sources Sci. Technol.* **23** 065016.
[3] Hontanon E et al. 2013 *J. Nanopart. Res.* **15** 1957.
[4] Hensel K et al. 2015 *Biointerphases* **10** 029515.
[5] Graves D B 2012 *J. Phys. D: Appl. Phys.* **45** 263001.
[6] Janda M at al. 2016 *Plasma Chem. Plasma Process.* **36** 767.

[7] Gaens W Van and Bogaerts A 2014 *Plasma Sources Sci. Technol.* **23** 035015.
[8] Jenista J 1999 *J. Phys. D: Appl. Phys.* **32** 2763.
[9] Barni R et al. 2005 *J. Appl. Phys.* **97** 073301.
[10] Flitti A and Pancheshnyi S 2009 *Eur. Phys. J.: Appl. Phys.* **45** 21001.
[11] Janda M, Hensel K and Machala Z 2018 *J. Phys. D: Appl. Phys.* **51** 334002.
[12] Gerling T et al. 2013 *Plasma Sources Sci. Technol.* **22** 065012.
[13] Janda M et al. 2017 *Plasma Sources Sci. Technol.* **26** 055010.
[14] Janda M et al. 2017 *J. Phys. D: Appl. Phys.* **50** 425207.
[15] Janda M et al. 2012 *Plasma Sources Sci. Technol.* **21** 045006.
[16] Pancheshnyi S et al. 2008 Computer Code ZDPlasKin, Univ. Toulouse, Toulouse, LAPLACE, CNRS-UPS-INP, France. [Online]. Available: https://www.zdplaskin.laplace.univ-tlse.fr
[17] Hagelaar G J M and Pitchford L C 2005 *Plasma Sources Sci. Technol.* **14** 722.
[18] LXCAT database. [Online]. Available: www.lxcat.net
[19] Marode E, Bastien F and Bakker M 1979 *J. Appl. Phys.* **50** 141.
[20] Naidis G V 2009 *Eur. Phys. J. Appl. Phys.* **47** 22803.
[21] Raizer Y P 1991 Gas Discharge Physics, *Springer-Verlag Berlin Heidelberg*.